On Modes of Tropical Circulation and Climate Anomalies

STEFAN HASTENRATH

Department of Meteorology, The University of Wisconsin, Madison 53706

(Manuscript received 20 May 1977, in final form 1 September 1978)

ABSTRACT

Large-scale departure maps of sea level pressure (SLP) and sea surface temperature (SST) are presented for the tropical Atlantic and eastern Pacific Oceans, as obtained by stratification with respect to extreme climatic events in key regions of the tropical Americas. Drought in the Central American-Caribbean region is characterized by an equatorward expansion of the North Atlantic high, a band of anomalously cold water extending across the North Atlantic and a positive SST anomaly in the eastern Pacific. Drought in northeast Brazil is associated with high SLP over the South Atlantic and low SLP over the North Atlantic, cold water in the South Atlantic, a band of positive SST anomalies across the North Atlantic, and positive SST departures in the eastern Pacific. During the Ecuador/Peru El Niño, SLP in the eastern Pacific is low and SST high, and positive SLP departures dominate the tropical Atlantic.

Independently, preferred modes of departure configurations are identified from principal component analysis of SLP (1942–71) and SST (1948–71). The first four principal components of SLP explain 43, 26, 14 and 10%, and the first four SST components 42, 24, 10 and 6% of the variance. The first principal components of SLP and SST, and the sea temperature along the Ecuador/Peru coast are highly correlated. This ensemble of departure configurations closely replicates the ones characteristic of the Ecuador/Peru El Niño. The second principal components of SLP and SST are correlated, as is the third SLP with the fourth SST component. However, the departure patterns obtained by stratification with respect to regional climate anomalies provide no overall analogy to these pattern ensembles. The fourth principal SLP and the third SST components are highly correlated. Both possess a high correlation of one sign with rainfall in the Central American-Caribbean region, and a high correlation of opposite sign with precipitation in northeast Brazil. This pattern ensemble offers an excellent replication for the two sets of departure patterns obtained by stratification with respect to drought in the Central American-Caribbean region and northeast Brazil. An additional principal component analysis was performed in which SLP, SST, and the three aforementioned regional hydrometeorological time series simultaneously served as input. Results corroborate the separate SLP and SST principal component analyses.

The stratification and principal component analyses are complementary approaches, in that they yield realistic and physically plausible patterns. It is hypothesized that mass exchanges on the scale of the near-global tropics dominate the pressure pattern and are related to regional circulation changes and climate anomalies.

1. Introduction

Variations in the large-scale circulation of atmosphere and ocean concomitant with regional extreme events are of central concern in the dynamics of climate. Following Hildebrandsson (1897), Walker first studied extensively the long-term pressure oscillations on a near-global scale (Walker and Bliss, 1932, 1937). Berlage (1957, 1966) concentrated on the "Southern Oscillation," defining it as an exchange of air between centers in the eastern South Pacific and the Indonesian-North Australian area, with a time scale of the order of one to five years. A nodal line was found in the South American sector, with pressure variations over the South Atlantic being broadly out of phase with the eastern South Pacific and in phase with Indonesia. Berlage (1966) also noted the tendency for the warm water El Niño events off the Ecuador/Peru coast to occur concurrently with low pressure over the eastern South Pacific. Bjerknes (1966, 1969) postulated linkages between the Southern Oscillation, equatorial sea temperature anomalies, the thermally direct "Walker cell" along the Pacific Equator, and the extratropical circulation. Quinn (1974) exploited the Southern Oscillation for the prediction of the El Niño. Wyrtki (1975), Hurlburt *et al.* (1976), McCreary (1976) and Barnett (1977) explained the appearance of the warm water characteristics of the El Niño in terms of an oceanic response to the relaxation of wind stress over the open equatorial Pacific; this in turn resulting from the altered pressure distribution related to the Southern Oscillation. Alexander *et al.* (1974) drew attention to the relation between the Indian monsoon rainfall and the Southern Oscillation, good monsoons coinciding with low/high pressure in the realm of Indonesia/Easter Island.

Large-scale mass exhanges of the Southern Oscillation type encompassing the Southern Atlantic were also

0022-4928/78/2222-2231$05.00

found to be a factor in extreme climatic events in the Atlantic sector (Hastenrath and Heller, 1977; Markham and McLain, 1977), and in the positive coupling between the northeast Brazil Sêcas and the Ecuador/Peru El Niño in particular (Hastenrath and Heller, 1977; Covey and Hastenrath, 1978). Long-term pressure variations on the equatorward side of the North Atlantic high show an affinity to the quality of the rainy season in both the Central American-Caribbean region and Subsaharan West Africa (Hastenrath, 1976; Lamb, 1978a,b).

The present study shall focus on preferred pattern configurations of atmospheric-oceanic fields, characteristic of climatic hazards in three regions of the tropical Americas, namely, the Sêcas of northeast Brazil, the Ecuador/Peru El Niño, and extreme events in the Central American-Caribbean region. Variations of the general circulation associated with these regional climate "anomalies" have been studied previously (Hastenrath, 1976; Hastenrath and Heller, 1977; Convey and Hastenrath, 1978), and characteristic departure patterns of key fields over the open ocean were obtained by stratification. This approach shall here be complemented by the identification of preferred modes of departure patterns through principal component analysis.

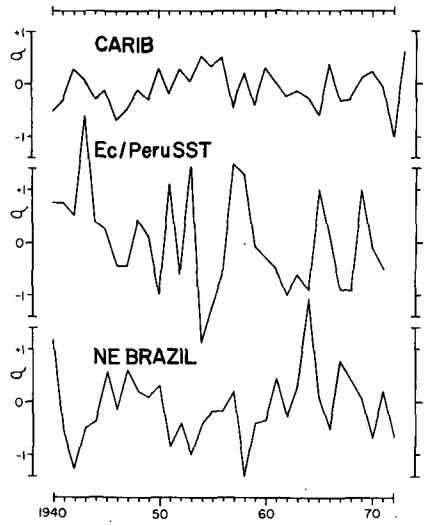

FIG. 1. Normalized departures of hydrometeorological indices plotted in terms of standard deviation. CARIB calendar-year rainfall totals at 48 stations in the Central American-Caribbean region; Ec/Peru SST, calendar-year average SST along the coast of Ecuador and Peru, composited from ship observations in area 0–10°S, 78–82°W, and measurements at ports of La Libertad, Puerto Chicama, Chancay; and NE BRAZIL, 12-month precipitation totals centered on March/April at 40 stations in northeast Brazil.

2. Observations and data processing

The observational basis of the project has been described in detail elsewhere (Hastenrath, 1976; Hastenrath and Heller, 1977; Hastenrath and Lamb, 1977). Ship data comprising more than 7 million sets of individual observations for the period 1911–72 were obtained on magnetic tape from the National Climatic Center at Asheville, NC. These were in the form of individual monthly averages of various meteorological parameters in 1° square areas of the tropical Atlantic and eastern Pacific Oceans (30°N to 30°S). Elements of interest here are sea level pressure (SLP) and sea surface temperature (SST). With the aim of compacting the information and enhancing data stability, time series of SLP and SST were compiled from this data bank for large ocean areas. SLP time series were constructed for six 10° latitude zones of the Atlantic. A finer spatial resolution into 25 ocean blocks seemed warranted for SST. The areas were delineated based on our earlier experience with climatic mean and anomaly patterns. The blocks are identified in the various maps to be discussed later (Figs. 3–4, 6–9).

SLP time series derived from ship observations are adequate for large ocean blocks of the tropical Atlantic, but data are deficient for the eastern Pacific. Alternatively, a pressure series for the years 1942–72 at Easter Island in the eastern South Pacific was obtained through the courtesy of Dr. W. Quinn. A time series of SLP at the axis of the North Pacific high for the years 1911–72 was compiled from microfilmed surface pressure maps obtained from the National Climatic Center.

In the course of our earlier work on climate dynamics, various areally representative and stable hydrometeorological time series of annual values have been constructed for key tropical areas (Hastenrath, 1976; Hastenrath and Heller, 1977; Covey and Hastenrath, 1978). The following three series are of interest here. Normalized departures of calendar-year rainfall totals were composited for 48 stations in the Central American-Caribbean region (CARIB). A similar time series of a hydrometeorological index was constructed from normalized departures of 12 month precipitation totals of 40 stations in northeast Brazil (NE BRAZIL), the 12-month intervals being centered on the peak of the rainy season in March/April. Values are ascribed to the calendar year containing the rainy season peak. A time series of an index of SST off the Ecuador/Peru coast (Ec/Peru SST) was constructed from calendar-year averages of SST at the ports La Libertad, Puerto Chicama and Chancay, and ship observations in the coastal strip 0–10°S, 78–82°W. Half of the weight was assigned to the ship observations, and the other half to the average of the port data. The compositing scheme seems adequate for the present purposes, although other weighting schemes are conceivable. The former two time series, CARIB and NE BRAZIL, provide a measure of extreme climatic events in two key land areas of the tropical Americas, and the series Ec/Peru SST pinpoints El Niño/counter-El Niño situations. Time series of these indices are displayed in Fig. 1.

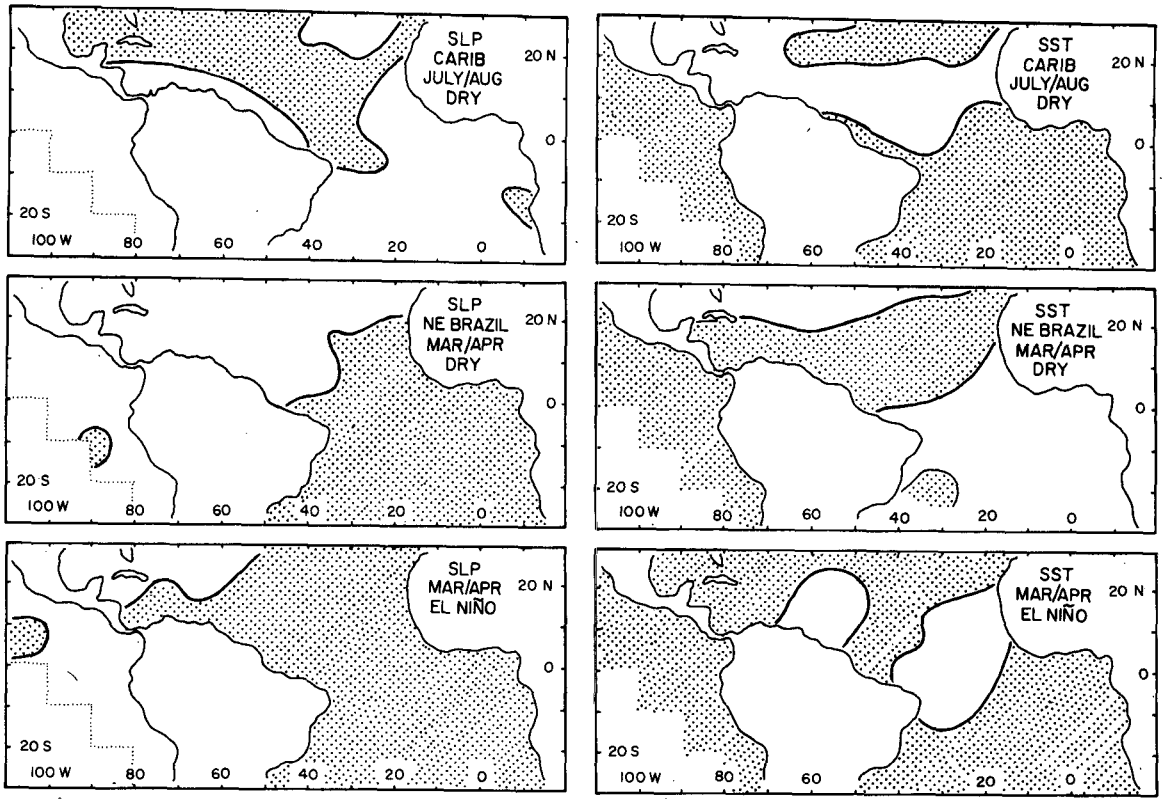

FIG. 2. Schematic maps of SLP and SST departure patterns obtained by stratification with respect to drought in the Central American-Caribbean area, drought in northeast Brazil and Ecuador/Peru El Niño. Positive areas are stippled.

Principal component analysis was applied to the aforementioned ensembles of SLP and SST time series. Input was in the form of calendar-year annual mean values. For a description of the technique reference is made to Kutzbach (1967) in particular. More recent applications to meteorology and oceanography are due to Kidson (1975) and Davis (1976). Principal components are a set of orthogonal functions each depicting a prominent pattern from the data, with disproportionately more variance explained by the first few components. The principal components can often be related to other fields of data, casting light on possible relationships of physical significance.

3. Large-scale departure patterns by stratification

Departure patterns of key parameters over the open oceans characteristic of Sêcas and their antithesis in northeast Brazil, drought/flood in the Central American-Caribbean region and Ecuador/Peru El Niño/counter El-Niño were constructed by stratification (Hastenrath, 1976; Hastenrath and Heller, 1977; Covey and Hastenrath, 1978). To this end, ten years of most extreme regional anomaly of either sign during 1911–72 were composited. For convenient reference, schematic maps of selected SLP and SST departure are reproduced in Fig. 2. Departures were tested in terms of Gaussian and binomial probabilities. The two complementary tests yielded probabilities of the order of 70 to more than 95% for the prominent departures. For details reference is made to the earlier work (Hastenrath, 1976; Hastenrath and Heller, 1977; Covey and Hastenrath, 1978).

Drought in the Central American-Caribbean region (Hastenrath, 1976) is characterized by an equatorward expansion of the North Atlantic high, a band of anomalously cold water across the North Atlantic and a positive SST anomaly in the eastern Pacific (Fig. 2).

Sêcas in northeast Brazil (Hastenrath and Heller, 1977) are associated with high pressure over the South and low pressure in the North Atlantic, negative SST departures in the South Atlantic and a zonally oriented warm water band in the North Atlantic.

The Ecuador/Peru El Niño (Covey and Hastenrath, 1978) is notorious for anomalously low pressure and high SST in the eastern Pacific. A further characteristic feature is the positive SLP anomaly in the tropical Atlantic.

Departure configurations associated with abundant rainy seasons in the Central American-Caribbean region and in northeast Brazil, and Ecuador/Peru counter-El Niño years are approximately inverse to the ones depicted in Fig. 2. As a rule, characteristic departure patterns are already apparent about half a year in advance. However, initial Ecuador/Peru El

Niño years tend to be preceded by inverse departure patterns.

4. Principal component patterns of pressure

Patterns of the first four principal SLP components (non-normalized) explaining 43.4, 26.4, 14.3 and 9.6% of the total variance, respectively, are shown in Fig. 3. Plots of the first four principal components in time series form are shown in Fig. 5.

The first principal SLP component is characterized by inverse anomalies in the Pacific and Atlantic, respectively, with particularly large amplitudes over the Southern Oceans. The second principal component reflects variations of the same sign in the entire map area, although with largest values over the Southern Oceans. This suggests a mass exchange with other parts of the globe. The third principal component represents mainly inverse pressure variations over the

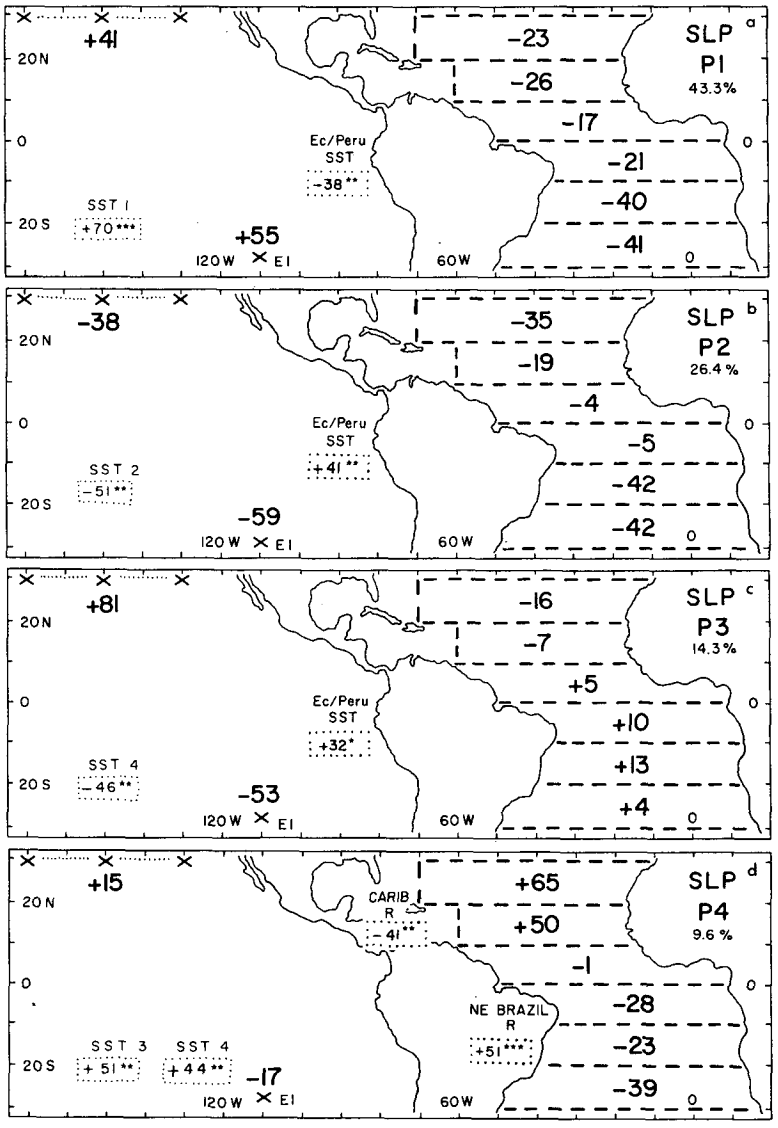

FIG. 3. Patterns of first four principal components (nonnormalized) of SLP pattern (P1, P2, P3, P4) explaining 43.3, 26.4, 14.3 and 9.6% of the variance, respectively. Dashed lines indicate ocean blocks for which SLP time series were compiled from ship observations. Axis of North Pacific high and Easter Island are marked by crosses. Bold numbers denote factor loadings in hundredths. Small numbers in dotted boxes are correlation coefficients, in hundreths, of principal SLP component pattern with key hydrometeorological time series and principal SST components; one, two and three asterisks denote significance at the 10, 5, and 1% levels, respectively. Period 1942–71.

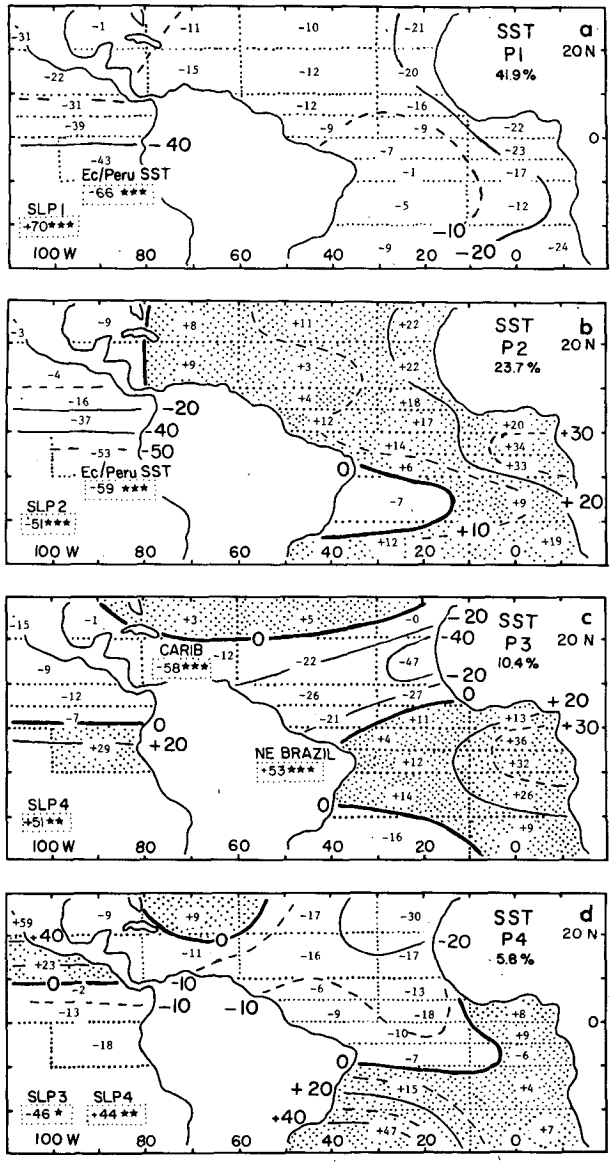

FIG. 4. As in Fig. 3 except for SST pattern, P1, P2, P3, P4, explaining 41.9, 23.7, 10.4, and 5.8% of the variance, respectively. Dotted lines indicate ocean blocks for which SST time series were compiled from ship observations. Numbers in ocean blocks and at isopleths (solid and dashed lines) denote factor loadings in hundredths. Positive areas are stippled. Small numbers in dotted boxes are correlation coefficients, in hundredths, of principal SLP component pattern with key hydrometeorological time series and principal SLP components; one, two and three asterisks denote significance at the 10, 5, and 1% levels, respectively. Period 1948–71.

eastern North and South Pacific. The sign of variations in the South and equatorial Atlantic is the same as for the eastern South Pacific, but amplitudes are small. The fourth principal component is characterized by variations of large amplitude in the North Atlantic and anomalies of opposite sign and lesser magnitude in the South Atlantic. It is realized that the analysis weights the Atlantic more heavily than the Pacific, because of the different number of time series used as input. The fact that large factor loadings appear in the Pacific underlines the importance of Pacific SLP variations.

5. Principal component patterns of sea temperature

Patterns of the first four principal SST components (non-normalized) explaining 41.9, 23.7, 10.4 and 5.8% of the total variance, respectively, are shown in Fig. 4. Plots of the first four principal components in time series form are shown in Fig. 5.

The first principal SST component reflects variations of the same sign in the entire map area, but with particularly large values in the eastern Pacific. The second principal component shows large anomalies of one sign in the eastern Pacific, but moderate departures of opposite sign in most of the tropical Atlantic. The third principal component is characterized by a broad band with strong anomalies of one sign extending across the tropical North Atlantic and moderate departures of opposite sign in most other portions of the map. It is again noted that the number of time series used as input assigns greater weight to the Atlantic than the Pacific.

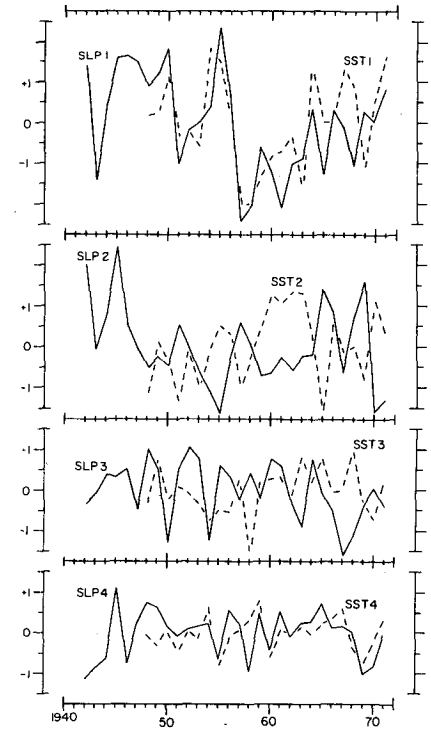

FIG. 5. Time series plots of the first four principal components (non-normalized) of pressure, SLP 1, SLP 2, SLP 3, SLP 4, solid, and of sea temperature SST 1, SST 2, SST 3, SST 4, dashed.

6. Coupling of pressure and sea temperature patterns and regional climate anomalies

As a measure of the linkage between large-scale departure patterns and regional climate anomalies, correlation coefficients were calculated between the time series of principal SLP and SST components and of the regional hydrometeorological indices. In estimating the significance of correlation coefficients, Quenouille's (1952, p. 168) method was used to account for the reduction of effective degrees of freedom due to persistence. The correlations between the principal SLP and SST components are presented in Table 1. Tables 2 and 3 show the correlations between the regional hydrometeorological indices and the principal components of SLP and SST, respectively. The most important correlations are also entered in Figs. 3 and 4 for convenience. The time series plots of Fig. 5 further permit a direct comparison of the march of the SLP versus the SST principal components.

The first principal component patterns of SLP and SST are highly correlated (Figs. 3a, 4a, 5, Table 1). Both are also highly correlated with Ec/Peru SST (Tables 2 and 3). Comparison of Figs. 3 and 4 with Fig. 2 shows that the first principal components of SLP and SST are a close replication of patterns obtained by stratification with respect to the Ecuador/Peru El Niño.

The second principal components of SLP and SST are also highly correlated (Figs. 3a, 4a, 5, Table 1). Both are highly correlated with Ec/Peru SST (Tables 2 and 3). The departure configurations obtained by stratification with respect to three kinds of regional climate anomalies (Fig. 2) offer no analogy to the overall patterns of the second principal components of SLP and SST. It is noted, however, that low SLP and high SST in the eastern Pacific appear concomitantly in the second principal components as for the Ecuador/Peru El Niño.

The third principal SLP and the fourth SST components are correlated (Figs. 3a, 4d, Table 1) but only the former is correlated with Ec/Peru El Niño (Tables 2, 3). Departure patterns by stratification (Fig. 2) provide no analogy except for low SLP over the eastern South Pacific being associated with the El Niño.

The fourth principal component of SLP is highly correlated with the third SST component (Figs. 3d, 4c, Table 1). Both possess a high correlation of one sign with CARIB, and a high correlation of opposite sign with NE BRAZIL. The fourth principal SST component has correlations of opposite sign with the third and fourth SLP component. The ensemble of the fourth principal SLP and the third SST components provide an excellent replication of two departures configurations displayed in Fig. 2, namely, the ones obtained by stratification with respect to extreme climatic events in the Central American-Caribbean region and northeast Brazil, respectively.

7. Combined principal component analysis

As discussed in Section 6, there is a close coupling between the principal components of SLP and SST, and regional climate anomalies. In order to further substantiate the linkages, an additional principal component analysis (normalized) was performed, using simultaneously as input SLP, SST, and the regional hydrometeorological time series. In the following this run shall be referred to as the *combined* principal component analysis. Results are presented in Figs. 6–9 in map form. SLP and SST patterns are depicted in separate charts, with the component loadings of CARIB, Ec/Peru SST and NE BRAZIL being plotted along with those of SLP. Fig. 10 is a time series plot of the first four components of the combined run. Correlation coefficients with the principal SLP and SST

TABLE 1. Correlation coefficients (10^{-2}) between principal components of SLP, P1, P2, P3, P4, and principal components of SST, P1, P2, P3, P4, period 1948–71; non-normalized. One, two and three asterisks denote significance at the 10, 5 and 1% levels, respectively.

SST	SLP			
	P1	P2	P3	P4
P1	+71***	−40*	−24	+15
P2	−0	−51**	−5	−19
P3	−17	+34	−16	+51**
P4	−19	−9	−46**	+44**

TABLE 2. Correlation coefficients (10^{-2}) between principal components (non-normalized) of SLP, P1, P2, P3, P4, and hydrometeorological time series from key tropical regions, CARIB, Ec/Peru SST, NE BRAZIL, (section 2), period 1942–71. Symbols as for Table 1.

	SLP			
	P1	P2	P3	P4
CARIB	+15	−26	−2	−41**
Ec/Peru SST	−38**	+41**	+32*	−26
NE BRAZIL	+17	−2	−17	+51***

TABLE 3. Correlation coefficients (10^{-2}) between principal components (non-normalized) of SST, P1, P2, P3, P4, and hydrometeorological time series from key tropical regions, CARIB, Ec/Peru SST, NE BRAZIL, (section 2), period 1948–71. Symbols as for Tables 1 and 2.

	SST			
	P1	P2	P3	P4
CARIB	+25	+28	−58***	−20
Ec/Peru SST	−66***	−59***	−6	−17
NE BRAZIL	+41*	+1	+53***	+3

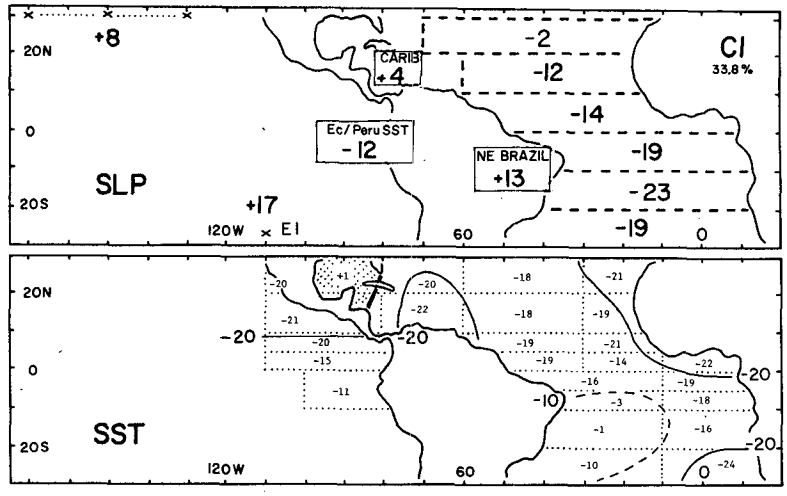

FIG. 6. Pattern of first component, explaining 33.8% of variance. Combined principal component analysis (normalized), using as input SLP, SST, CARIB (rainfall), NE BRAZIL (rainfall) and Ec/Peru SST (sea temperature). Period 1948–71. Symbols as in Figs. 3 and 4.

components of the separate runs (Sections 3 and 4) are listed in Table 4. Correlation coefficients with the regional hydrometeorological time series are also given, although these were part of the input into the combined analysis.

The first principal component pattern of the combined analysis (Fig. 6) is characterized by inverse SLP anomalies in the two oceans; by SST loadings in the entire map area being of opposite sign to the ones of SLP in the Pacific; and by having loadings of the sign opposite to those of Pacific SLP. This anomaly configuration is similar to the ensemble of the first principal SLP and SST component patterns in the separate analyses (Figs. 3a, 4a) and the concomitant Ec/Peru SST anomalies (Tables 2, 3). Accordingly, the time series plot of the combined analysis (Fig. 10) essentially parallels those of the principal SLP and SST components in the separate analyses (Fig. 5), and the correlations between these series are high (Table 4).

The second principal component of the combined analysis (Fig. 7) has SLP anomalies of different sign in the North and Equatorial Atlantic, and the rest of the map area, respectively; prominent SST anomalies, extending in a broad band across the northern equatorial Atlantic are of a sign opposite to that of SLP in the North Atlantic; and CARIB shows a factor loading of sign opposite to North Atlantic SLP. This anomaly configuration is similar to the ensemble of the fourth SLP and the third SST principal component patterns in the separate analyses (Figs. 3d, 4c), and the concomitant CARIB anomalies (Tables 2, 3). The time series plot of the combined analysis (Fig. 10) resembles

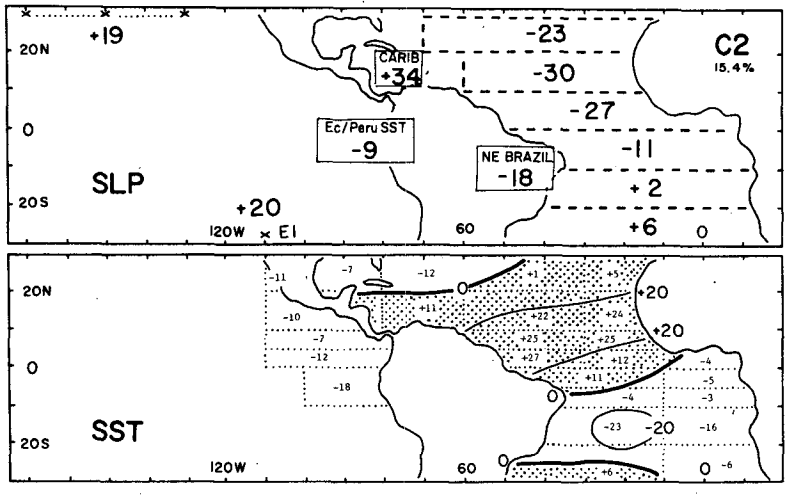

FIG. 7. Pattern of second component, explaining 15.4% of variance. Combined principal component analysis (normalized), using as input SLP, SST, CARIB, NE BRAZIL and Ec/Peru SST. Period 1948–71. Symbols as in Fig. 6.

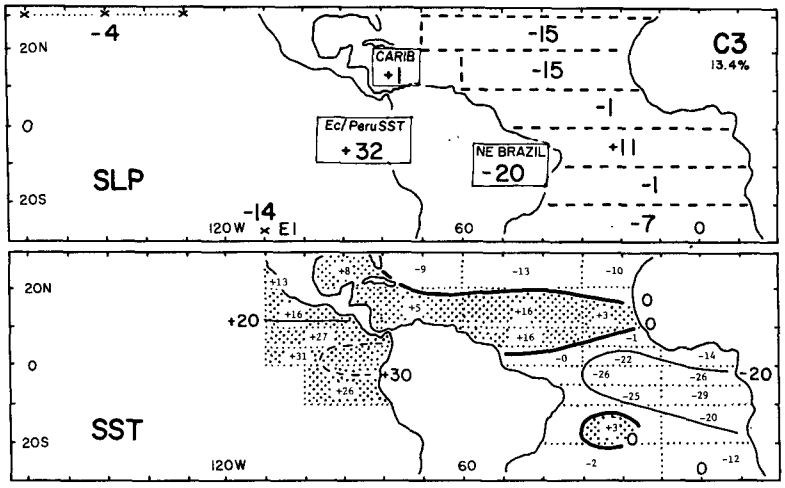

FIG. 8. Pattern of third component, explaining 13.4% of variance. Combined principal component analysis (normalized), using as input SLP, SST, CARIB, NE BRAZIL and Ec/Peru SST. Period 1948–71. Symbols as in Fig. 6.

those of the fourth SLP and the third SST principal components in the separate analysis (Fig. 5). The high correlations between these time series and with CARIB are also borne out by Table 4.

The third principal component of the combined analysis (Fig. 8), is characterized by SLP and SST anomalies of opposite sign in the Pacific. SLP anomalies in the equatorial Atlantic are opposite to those in the Pacific, but of the same sign as SST anomalies in a zonally oriented band of the equatorial North Atlantic. Furthermore, the loading of Ec/Peru SST has a sign opposite to Pacific SLP and NE BRAZIL. This anomaly configuration bears some resemblance to the ensemble of the second SST and SLP principal component patterns in the separate analyses (Figs. 4b, 3b), and the concomitant anomalies of Ec/Peru SST (Tables 2, 3). This resemblance is further illustrated by the comparison of time series plots in Figs. 5 and 10, and the correlation coefficients in Table 4. In fact, the inverse relationship of patterns characteristic of Ecuador/Peru El Niño and northeast Brazil Sêcas as illustrated in Fig. 2 is rather more clearly replicated in the combined as compared to the separate principal component analyses.

The fourth principal component of the combined analysis is also shown for completeness (Fig. 9), although the charts do not replicate patterns known from the separate SLP and SST principal component analyses, or the departure maps constructed by stratification. This lack of relationship is also indicated by the time series plots (Figs. 5 and 10) and the correlation coefficients in Table 4.

In broad terms, the combined principal component analysis complements the separate SLP and SST runs

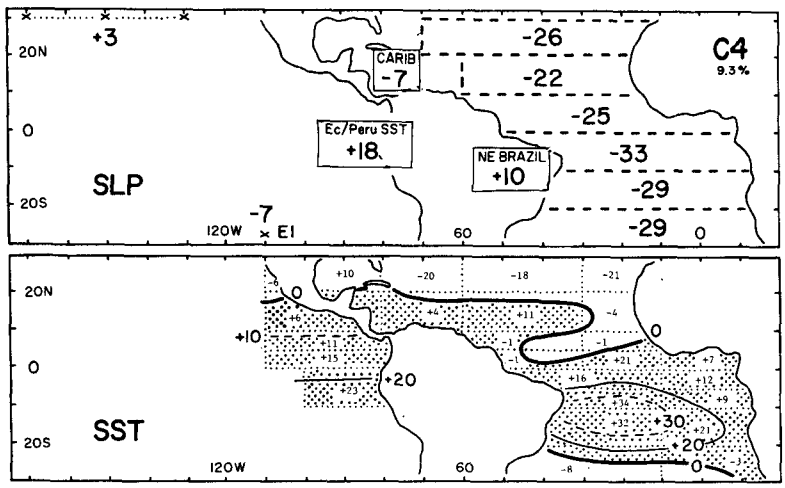

FIG. 9. Pattern of fourth component, explaining 9.3% of variance. Combined principal component analysis (normalized), using as input SLP, SST, CARIB, NE Brazil and Ec/Peru SST. Period 1948–71. Symbols as in Fig. 6.

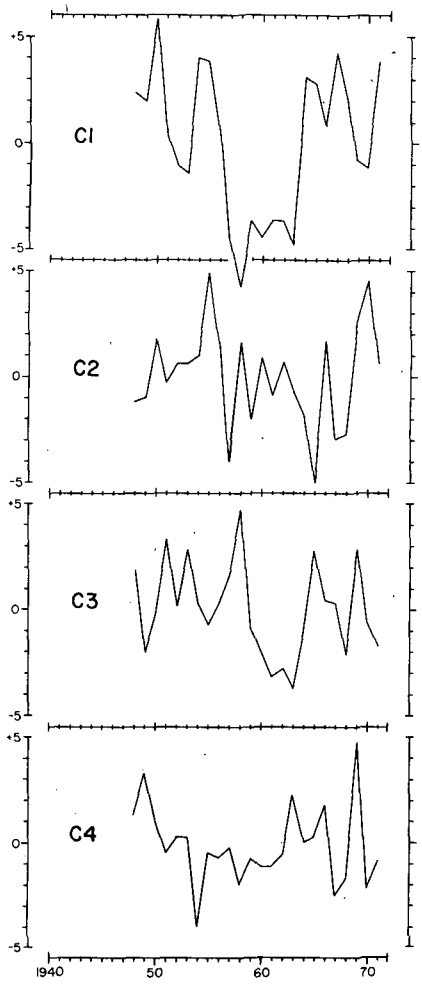

FIG. 10. Time series plots of the first four components P1, P2, P3, P4 from combined principal components analysis (normalized), using as input SLP, SST, CARIB, NE BRAZIL and Ec/Peru SST.

discussed in Sections 3–6. Considering the number of time series used as input it is realized that SST should dominate the pattern more strongly than SLP. In particular, the three regional hydrometeorological indices enter with disproportionately small weight. The fact that they nonetheless appear with large loadings in certain principal components of the combined analysis illustrates their relative importance.

8. Conclusions

An inventory of large-scale atmospheric and oceanic departure patterns characteristic of regional extreme events is fundamental in the search for general circulation mechanisms of climate anomalies. In the present project departure patterns associated with rainfall and SST anomalies in key tropical regions were first constructed by stratification. Independently preferred modes of pattern configurations were identified by principal component analysis. The two approaches are

TABLE 4. Correlation coefficients (10^{-2}) between principal components (normalized) of combined run (having as input SLP, SST, and the three regional hydrometeorological time series), C1, C2, C3, C4 and the principal components (non-normalized) of pressure, SLP 1, SLP 2, SLP 3, SLP 4; the principal components (non-normalized) of sea temperature, SST 1, SST 2, SST 3, SST 4; and CARIB, Ec/Peru SST, and NE BRAZIL; period 1948–71. One, two, three and four asterisks denote significance at the 10, 5, 1 and 0.1% levels, respectively.

	C1	C2	C3	C4
SLP 1	+74***	+49**	−10	+27
SLP 2	−13	−42**	+40*	+51**
SLP 3	−27	+16	+17	+12
SLP 4	+26	−67****	−22	+6
SST 1	+91****	+16	−24	−25
SST 2	−33	+40*	−81****	−17
SST 3	+10	−67****	−49**	+37*
SST 4	0	−40*	−2	−36*
CARIB	+12	+81****	+2	−13
Ec/Peru SST	−42*	−21	+70****	+32
NE BRAZIL	+45*	−44**	−44*	+18

complementary in that realistic and mutually compatible patterns were obtained. Although stratification and principal component analysis do not establish physical causalities as such, they permit an appraisal of hypotheses of mechanisms of circulation and climate change.

It is largely to the credit of the NORPAX effort (review in the Introduction) that a chain of physical causalities is now understood as linking the Southern Oscillation pressure see-saw of the great Pacific basin with buildup and relaxation of wind stress, SST and rainfall anomalies in the equatorial belt, and the regional manifestations of the Ecuador/Peru El Niño. The modes of inverse SLP and SST departures in the eastern Pacific found in the present study (Figs. 2, 3a,b, 4a,b, 5, 8) are consistent with this physical mechanism.

The present work further substantiates an SLP see-saw of the Southern Oscillation type in the zonal direction, with inverse SLP departures over the southern and equatorial Atlantic and eastern Pacific, respectively (Figs. 2, 3, 6). Our earlier work (Hastenrath and Heller, 1977) has also shown that long-term pressure variations on the equatorward flank of the South and North Atlantic highs are associated with the meridional shifts of the equatorial wind regimes and related surface confluence axis and convergence band. The rainy season in northeast Brazil is narrowly centered around March/April, concomitant with the southernmost seasonal migration of the quasi-permanent convergence band over the Atlantic. The Sêcas of northeast Brazil appear related to an anomalously far northerly position of the convergence band, a phenomenon which is found associated with SLP anomalies over the South Atlantic. These in turn tend to run inverse to the eastern Pacific. This SLP see-saw between the two Southern

Oceans is suggested as a cause for the coupling of the northeast Brazil Sêcas and the Ecuador/Peru El Niño. The preferred departure modes identified here seem compatible with the physical mechanisms proposed for the origin of climatic hazards in northeast Brazil and their coupling with events in the Pacific.

It is surmised that deficient/abundant rainy seasons in the Central American-Caribbean area are directly related to an alteration of the divergence pattern, although this cannot be substantiated quantitatively from existing data. The divergence pattern in turn is presumably affected by changes in the long-term pressure distribution. For example, an equatorward expansion of the North Atlantic high is expected to enhance divergence in the Caribbean domain, thus leading to a deficient rainy season. The aforementioned tendency for inverse SLP departures in the Atlantic and Pacific may be causally related to the coupling of the Central American-Caribbean drought and Ecuador/Peru El Niño. The departure ensembles found here (Figs. 2, 3d, 4c, 5, 7) seem compatible with the chain of causality outlined above. The causal linkage between SLP departures on the equatorward side of the North Atlantic high and concomitant inverse SST anomalies in the equatorial North Atlantic may be elucidated in part by an investigation of phase relationship. This shall be studied at a later time.

In conclusion, large-scale mass exchanges in the zonal direction appear to play a dominant role in the creation of anomalous pressure patterns over the oceans surrounding the tropical Americas, as well as in other sectors of the tropics. Altered pressure distributions spanning a large part of the globe appear concomitant with variations of wind, divergence and SST fields on the scale of individual oceans. The latter features in turn may relate directly to regional rainfall anomalies. For an understanding of regional climate anomalies complementary analyses appear called for, encompassing both the regional scale of hundreds to thousands kilometers and the scale of the near-global tropics.

Acknowledgments. This study was supported by the National Science Foundation Climate Dynamics Research Program. I thank Peter Guetter for the use of his principal component program, and John Kutzbach and Wayne Wendland for comments on draft versions of this paper.

REFERENCES

Alexander, G., R. N. Keshavamurty, R. K. Mikhopadhyay, and S. G. Bhosale, 1974: Pacific equatorial pressure gradient and Indian monsoon rainfall. *Nature*, **252**, 463–464.

Barnett, T. P., 1977: An attempt to verify some theories of El Niño. *J. Phys. Oceanogr.*, **7**, 633–647.

Berlage, H. P., 1957: Fluctuations of the general circulation of more than one year, their nature and prognostic value *Konink. Neder. Meteor. Inst. Meded. Verhand.*, No. 102–69, 152 pp.

——, 1966: The Southern Oscillation and world weather. *Konink. Neder. Meteor. Inst. Meded. Verhand.*, No. 102–88, 152 pp.

Bjerknes, J., 1966: A possible response of the atmospheric Hadley circulation to equatorial anomalies of ocean temperature. *Tellus*, **18**, 820–829.

——, 1969: Atmospheric teleconnections from the equatorial Pacific. *Mon. Wea. Rev.*, **97**, 163–172.

Covey, D. L., and S. Hastenrath, 1978: The Pacific El Niño phenomenon and the Atlantic circulation. *Mon. Wea. Rev.*, **106**, 1280–1287.

Davis, R. E., 1976: Predictability of sea surface temperature and sea level pressure anomalies over the North Pacific Ocean. *J. Phys. Oceanogr.*, **6**, 249–266.

Hastenrath, S., 1976: Variations in low-latitude circulation and extreme climatic events in the tropical Americas. *J. Atmos. Sci.*, **33**, 202–215.

——, and L. Heller, 1977: Dynamics of climatic hazards in northeast Brazil. *Quart. J. Roy. Meteor. Soc.*, **103**, 77–92.

——, and P. Lamb, 1977: *Climatic Atlas of the Tropical Atlantic and Eastern Pacific Oceans*. University of Wisconsin Press, 105 pp.

Hildebrandsson, H., 1897: Les centres d'action de l'atmosphère. *Kongl. Svenska Veten.-Akad. Handl.*, **29**, No. 3, 36 pp.

Hurlburt, H. E., J. C. Kindle and J. J. O'Brien, 1976: A numerical simulation of the onset of El Niño. *J. Phys. Oceanogr.*, **6**, 621–631.

Kidson, J. W., 1975: Eigenvector analysis of monthly mean surface data. *Mon. Wea. Rev.*, **103**, 177–186.

Kutzbach, J. E., 1967: Empirical eigenvectors of sea level pressure, surface temperature and precipitation complexes over North America. *J. Appl. Meteor.*, **6**, 791–802.

Lamb, P., 1978a: Case studies of tropical Atlantic surface circulation patterns during recent sub-saharan weather anomalies: 1967 and 1968. *Mon. Wea. Rev.*, **106**, 482–491.

——, 1978b: Large-scale tropical Atlantic surface circulation patterns associated with subsaharan weather anomalies. *Tellus*, **30**, 240–251.

Markham, C. G., and D. R. McLain, 1977: Sea surface temperature related to rain in Ceará, northeastern Brazil. *Nature*, **265**, 320–323.

McCreary, J., 1976: Eastern tropical ocean response to changing wind system: with application to El Niño. *J. Phys. Oceanogr.*, **6**, 632–645.

Quenouille, M. H., 1952: *Associated Measurements*. Butterworths, London, 242 pp.

Quinn, W. H., 1974: Monitoring and predicting El Niño invasions. *J. Appl. Meteor.*, **13**, 825–830.

Walker, G. T., and E. W. Bliss, 1932: World Weather V. *Mem. Roy. Meteor. Soc.*, **4**, No. 36, 53–84.

——, and ——, 1937: World Weather VI. *Mem. Roy. Meteor. Soc.*, **4**, No. 39, 119–139.

Wyrtki, K., 1975: El Niño—the dynamic response of the equatorial Pacific Ocean to atmospheric forcing. *J. Phys. Oceanogr.*, **5**, 572–584.